



# Reliable thermodynamic estimators for screening caloric materials

Nikolai A. Zarkevich <sup>a,\*</sup>, Duane D. Johnson <sup>a,b</sup>

<sup>a</sup> Ames Laboratory, U.S. Department of Energy, Ames, IA, 50011-3020, USA

<sup>b</sup> Materials Science & Engineering, Iowa State University, Ames, IA, 50011-2300, USA



## ARTICLE INFO

### Article history:

Received 20 February 2019

Received in revised form

8 May 2019

Accepted 11 June 2019

Available online 15 June 2019

### Keywords:

caloric

Thermodynamic

Metamagnetic

Phase transformation

FeRh

## ABSTRACT

Reversible, diffusionless, first-order solid-solid phase transitions accompanied by caloric effects are critical for applications in the solid-state cooling and heat-pumping devices. Accelerated discovery of caloric materials requires reliable but faster estimators for predictions and high-throughput screening of system-specific dominant caloric contributions. We assess reliability of the computational methods that provide thermodynamic properties in relevant solid phases at or near a phase transition. We test the methods using the well-studied B2 FeRh alloy as a “fruit fly” in such a materials genome discovery, as it exhibits a metamagnetic transition which generates multicaloric (magneto-, elasto-, and baro-caloric) responses. For lattice entropy contributions, we find that the commonly-used linear-response and small-displacement phonon methods are invalid near instabilities that arise from the anharmonicity of atomic potentials, and we offer a more reliable and precise method for calculating lattice entropy at a fixed temperature. Then, we apply a set of reliable methods and estimators to the metamagnetic transition in FeRh (predicted  $346 \pm 12$  K, observed  $353 \pm 1$  K) and calculate the associated caloric properties, such as isothermal entropy and isentropic temperature changes.

© 2019 Elsevier B.V. All rights reserved.

## 1. Introduction

Solid-state caloric devices have a potential to save vast amounts of electricity [1–6]. However, predicting thermodynamics in a caloric material can be challenging [7], as near the phase transformation – where caloric effects are induced – the system is on the edge of stability, often with multiple instabilities competing. Hence, thermodynamic estimators need a serious assessment before applications to caloric systems [8], or for use in high-throughput screening supplemented using databases and machine-learning techniques.

The caloric effect is typically quantified by the isothermal entropy change  $\Delta S_T$  and associated isentropic temperature change  $\Delta T_S$  at the phase transition at a critical temperature  $T_c$ . But these are not the only important quantities. Others include the enthalpy change  $\Delta H$  at a fixed pressure  $P$  or temperature  $T$  (importantly,  $\Delta H_P \neq \Delta H_T$ ), the hysteresis width, dependences of  $T_c$  on composition and external fields, etc. Thus, a search for a good caloric material involves simultaneous optimization of multiple parameters. For their accurate prediction, it is important to take into account

several contributing physical effects, using multi-physics, multi-parameter modeling. On the other hand, quick estimates of the lower and upper bounds allow fast rejection, needed for the high-throughput materials screening.

Our key goal here is to test the reliability of various (often commonly used) methods and to validate our results with those that are measured. The overarching need is a set of reliable, and preferably fast, estimators for thermodynamic quantities for screening, especially for desired outliers – say, materials with a large caloric response. Such materials, however, have electronic (including magnetic) and structural instabilities, in which case the vibrational contributions are often not harmonic; and yet quasi-harmonic phonon methods are commonly used.

To analyze and test methods and estimates, we use the multicaloric FeRh system. With its chemical simplicity and well-studied metamagnetic transition, FeRh serves as a wonderful “fruit fly”, or test system, in the materials genome discovery of better caloric systems [9]. However, a long-studied material is not necessarily well understood; there is a continued controversy among the directly measured and indirectly assessed experimental data, as we discuss.

Interestingly, FeRh [10–14] and NiTi austenite [15–18] have the same nominal chemical B2 structure (CsCl,  $Pm\bar{3}m$  space group, see Fig. 1) and exhibit a large caloric effect [19–24]. Both B2 austenites (FeRh below 353 K and NiTi above 313 K) have a premartensitic

\* Corresponding author.

E-mail addresses: [zarkev@ameslab.gov](mailto:zarkev@ameslab.gov) (N.A. Zarkevich), [ddj@iastate.edu](mailto:ddj@iastate.edu), [ddj@ameslab.gov](mailto:ddj@ameslab.gov) (D.D. Johnson).

instability with known unstable phonon modes [16,17]. While they both show elasto- and baro-caloric responses, FeRh also exhibits a giant magnetocaloric effect at its metamagnetic transition from an antiferromagnetic (AFM) to a ferromagnetic (FM) state at the critical temperature  $T_c$  of 353 K, with a 1% decrease in density [14]. Properties of FeRh were extensively studied experimentally [12–14,19–21,25–46] and theoretically [22,47–61]. Notably, the metamagnetic  $T_c$  of FeRh is sensitive to stoichiometry, lowering precipitously with small additions of at.%Rh [29]. A giant caloric effect is found at this transition in the quenched Fe<sub>49</sub>Rh<sub>51</sub> sample [19], i.e., a directly measured temperature drop of 12.9 K at 1.95 Tesla.

While bulk FeRh is prohibitively expensive, Fe–Rh may find use in caloric thin-film [19,21,36,44,62–70] and nanoscale devices [43,59,71–79]. Nonetheless, and notably here, it mainly serves as a well-studied but suitably complex system to test methods for reliability in thermodynamic assessments and prediction of caloric properties, specifically because it exhibits instabilities from anharmonic atomic motion, which affects caloric behavior. The FeRh groundstate and a martensitic transformation in the AFM phase at cryogenic temperatures were recently addressed [80].

Here we focus on estimators [8] to predict thermodynamics at the metamagnetic transformation near room temperature. We find that quantities relevant to calorics can be calculated in a quantitative agreement with measurements (Table 1). We also provide insight into the key requirements to predict caloric behavior accurately – necessary to identify the computational screening measures and correlations that assist in materials discovery [81]. While some computations can be intensive (e.g., phonons and lattice entropy), the results are useful for testing faster estimators [82–84].

Computational details are provided in section 2. In section 3, we address the caloric effects and calculate  $\Delta S_T$  and  $\Delta T_S$  at the metamagnetic transition. Importantly, in subsection 3.4 we test a method for addressing non-harmonic atomic vibrations at a relevant temperature, because the commonly-used linear-response and small-displacement methods employed to assess lattice entropy fail near lattice instabilities, including those that arise from anharmonicity of the atomic potential energy surface. In section 4, we offer estimators of enthalpy change  $\Delta H$ , transition temperature  $T_c$ , and its derivative  $dT_c/dB$  with respect to the external field  $B$ . Some of the issues and limitations of the common and alternative approaches are discussed in section 5. Generic remarks about the upper bounds, chemical disorder, and hysteresis are provided in section 6. In section 7, screening for better caloric systems beyond FeRh, as now verified experimentally, is presented, followed by a summary in section 8. Thus, we review and assess the relevant methods and estimates of caloric properties, as showcased in a test system (FeRh), but which may be applied quite generally.

## 2. Computational methods

For FeRh compound, density functional theory (DFT) calculations were performed using the Vienna *ab initio* simulation package

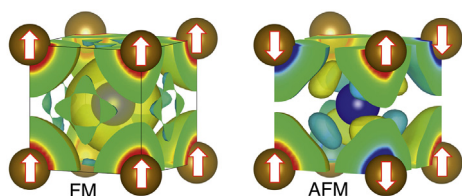


**Figure 1.** (Color online). In B2 FeRh, the electronic spin density as  $\pm 0.002 e/\text{\AA}$  iso-surfaces in (001) FM (left) and (111) AFM (right) spin configurations.

**Table 1**

Calculated (Theory) and experimental (Expt.) magnetization, lattice constant, caloric effect, and phase transition temperature. References are given for experiment.  $\Delta S$  differs from  $\Delta S_T(T_c)$  due to incorrect assessment [30,40], see sections 3.5 and 5.

	Theory	Expt.	Units	Ref.
$M$ (FM)	149	$\approx 150$	$\text{\AA m}^2 \text{kg}^{-1}$	[42]
$a$ (FM)	3.012	2.997	$\text{\AA}$	[14,30]
$a$ (AF)	2.996	2.987	$\text{\AA}$	[14,30]
$\Delta S_T(T_c)$	11.9	12–14	$\text{Jkg}^{-1} \text{K}^{-1}$	[12,21,65,85,86]
$\Delta S$		17–19	$\text{Jkg}^{-1} \text{K}^{-1}$	[22,30,40]
$-\Delta T_S$	13	10–13	K	[21,65]
$T_c$ (AF–FM)	346	353	K	[29]

(VASP) [87,88]. We used projector augmented waves (PAW) [89,90] and the PBE exchange–correlation functional [91] with Vosko–Wilk–Nusair spin-polarization [92], combined with a modified Broyden method [93] for accelerated convergence. Brillouin zone integrations were performed on a Monkhorst–Pack mesh [94] with  $\geq 50$   $k$ -points per  $\text{\AA}^{-1}$  with  $\Gamma$  included. The plane-wave basis-set energy cutoff was increased to 334.9 eV (or 511.4 eV for augmentation charges) by the high-precision flag. During computing of the atomic forces, an additional (third) support grid was used for the evaluation of the augmentation charges.

In non-stoichiometric cases, chemical disorder was addressed using either supercells or the coherent potential approximation (CPA) [95], implemented in the KKR code MECCA [96]. Components of the TTK toolkit [97] were used to prepare the supercells.

As needed for barriers or saddle-point transitions [80], DFT was combined with a generalized solid-state nudged elastic band (GSS-NEB) [98], which includes a built-in C2NEB algorithm [99] with two climbing images [100].

Phonons were calculated using the finite atomic displacement method, implemented in the Phon code [101]. The force-constant matrix [101] was constructed from the atomic forces (in the file FORCES), computed using VASP. The atomic displacements varied from 0.04 to 0.12  $\text{\AA}$  in a cubic  $4 \times 4 \times 4$  supercell containing 64 FeRh formula units (f.u.). The phonon density of states was computed [101] using  $21^3$   $k$ -point grid in the reciprocal space (LRE-CIP=.TRUE.) and the Gaussian smearing (DOSSMEAR = 0.05 THz); the output file THERMO provided the lattice entropy  $S_L$  at finite  $T$ . We used the experimental atomic masses:  $m(\text{Fe}) = 55.845$  and  $m(\text{Rh}) = 102.9055$  atomic unified mass units,  $u = \frac{1}{12} m(^{12}\text{C})$ . We also present a method that more properly addresses anharmonic vibration near instabilities, which has a significant affect on entropy.

## 3. Results

The magnetostructural transition in B2 FeRh between FM and AFM phases (Fig. 1) is accompanied by a change of electronic structure (Fig. 2), energy and volume (Fig. 3). While an electronic transition happens with the speed of light, a structural transformation (including volume change) propagates no faster than the speed of sound [102]. So, the electronic transformation is accompanied by discontinuity in pressure that drives the volume change [103]. The possible causes for electronic transitions include initial structure change or application of an external field. In particular, as is well established, the magnetostructural transformation of FeRh can be caused by application of an external magnetic field and/or stress, strain, or thermal expansion.

### 3.1. Spin density and itinerant magnetism

Fig. 1 shows the real-space distribution of the electronic spin

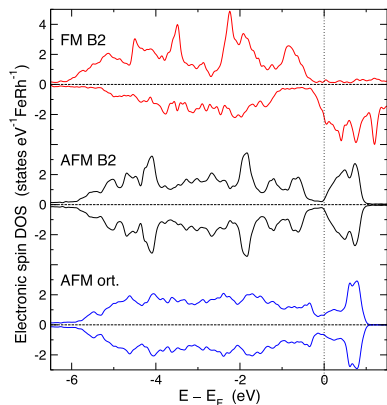


**Figure 2.** (Color online). For B2 FeRh, electronic DOS for FM (upper) and AFM spin ordering, and AFM orthorhombic structure (lower) at zero pressure [61].

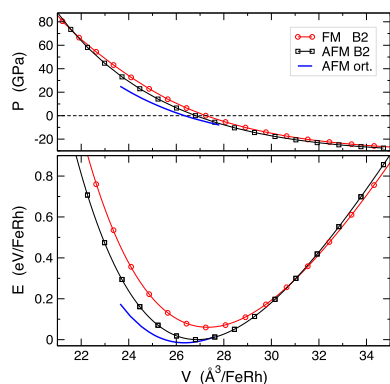


**Figure 3.** (Color online). Pressure  $P$  (GPa) and energy  $E$  (eV) vs. volume  $V$  ( $\text{\AA}^3$ ) per FeRh formula unit for B2 FM and AFM, and orthorhombic AFM structures.

density in the B2 cubic cell of FeRh, which is an itinerant magnet. Importantly, spin density around Rh atoms is not zero in both phases, but the atomic magnetic moment of Rh is zero in an ideal B2 AFM structure due to the inversion symmetry with a center at Rh nucleus. Indeed, if the distribution of Fe moments is symmetric in the AFM phase, then the electronic spin density sums to zero within the Rh atomic sphere (and within an arbitrary Rh-centered sphere of any radius). However, any asymmetry due to the fluctuating Fe–Rh distances or Fe moments (e.g., due to thermal disorder) would result in a non-zero atomic magnetic moment of Rh.

At the AFM–FM phase transition, the calculated magnetization changes from zero to  $149 \text{ Am}^2/\text{kg}$  ( $4.2 \mu_B/\text{FeRh}$ ). With caution, one can integrate the spin density inside each atomic sphere to find the “atomic” magnetic moment. We find that the Rh moments change from 0 (AFM) to  $1 \mu_B$  (FM), and the Fe moments change from  $\pm 3.1$  (AFM) to  $3.2 \mu_B$  (FM).

### 3.2. Electronic and magnetic entropy

As seen in Fig. 2, the total electronic spin density of states (DOS) at the Fermi energy  $E_F$  changes substantially during the transformation from  $n(E_F) = 0.677$  in the AFM to  $2.310$  states/eV per FeRh formula unit (f.u.) in the FM state. Contributions of both spins are equal in the AFM, while minority spins dominate at  $E_F$  in the FM state (Fig. 2).

The electronic entropy (as estimated by the Sommerfeld’s expansion) is

$$S_e(T) \approx \left(\pi^2/3\right) \cdot k_B^2 T \cdot n(E_F), \quad (1)$$

which yields  $0.23$  (FM) and  $0.07$  (AFM)  $k_B/\text{FeRh}$  at  $T_c$ . The difference  $\Delta S_e$  is  $0.163 k_B/\text{FeRh}$  (or  $0.08 k_B$  per atom). The Sommerfeld approximation in most cases tested has been a reasonably reliable approximation between structural variants arising at solid–solid phase transitions.

Spin-polarized electrons are responsible for both conductivity and magnetism; they account for both electronic and magnetic contributions to the entropy, as required in an itinerant magnet [82], such as FeRh. Fluctuations of atomic magnetic moments can be expanded in an electronic basis in both FM and AFM phases.  $S_e$  includes entropy of thermal excitations in both spin channels (i.e., electronic and magnetic contributions).

The total entropy is  $S = \ln \Omega$ , where  $\Omega$  is the number of accessible microstates in the whole system. Typically, magnetic entropy is small in the FM and AFM states, where the number of magnetic states (per atom) is close to 1, and it is larger in a paramagnetic (PM) state, which is not relevant to the AFM–FM phase transition. In decomposing the total entropy into electronic, magnetic, and lattice contributions, sometimes mistakes were made [40], leading to notably wrong findings.<sup>1</sup> We discuss the issues with indirect assessments in section 5.

### 3.3. Compression and expansion

The energy  $E$  and pressure  $P$  versus volume  $V$  curves for the main competing structures in FeRh are shown in Fig. 3. The FM B2 and AFM B2 are the terminal states of the metamagnetic phase transition, accompanied by the magnetocaloric effect; the AFM orthorhombic (martensitic) ground state of FeRh is discussed elsewhere [80]. The calculated equilibrium lattice constants  $a = V^{1/3}$  are compared to experiment in Table 1, less than +0.2% difference from experiment using a PBE density functional. The FM and AFM states have a crossover at higher volumes. From these plots, the metamagnetic transition already can be anticipated. At zero pressure  $P$ , the FM state is  $\delta H_0 = 29.8 \pm 1.0$  meV/atom above the AFM state ( $\delta H_0/k_B = 346 \pm 12$  K, i.e., near the measured  $T_c = 353$  K, see section 4).

In addition, a premartensitic instability is anticipated in B2 AFM state with known phonon instabilities [57–59], and a martensitic transformation from B2 AFM austenite to orthorhombic AFM martensite at cryogenic  $T$  was suggested by direct GSS-NEB calculations [61].

### 3.4. Lattice entropy – anharmonic and harmonic vibrations

Vibrational entropy in materials can contribute significantly to their caloric response. To assess vibrational entropy of phonon excitations at a finite  $T$ , the standard approach is to calculate the quasiharmonic phonon frequencies by linear-response or small atomic displacement method. However, both of these methods inherently assume a harmonic atomic potential. In materials with structural and magnetic instabilities (or, more generally, “dimpled” potential energy surfaces), this assumption is invalid, at least near temperatures, where the crossover between states occur and key associated properties manifest. With the premartensitic instability [80] in AFM(111) B2 FeRh, similar (but smaller) to that in NiTi

<sup>1</sup> In Ref. [40], the total integrated entropy difference ( $\Delta S = 17 \pm 3$  J/kg/K) was incorrectly decomposed into lattice ( $\Delta S_{\text{latt}} = -33 \pm 9$  J/kg/K), electronic ( $\Delta S_{\text{el}} = 8 \pm 1$  J/kg/K), and magnetic ( $\Delta S_{\text{mag}} = 43 \pm 9$  J/kg/K) contributions. The negative sign of the lattice contribution is notable.

austenite [16,17], care must be taken to calculate accurately the lattice entropy.

Here, distinct from previous work, we evaluate phonon frequencies and density of states (DOS) along with their sensitivity to the atomic displacement  $d$  used to calculate them. Using the small-displacement method [101] at zero pressure, we find an unstable phonon mode at  $M$  ( $\frac{1}{2}\frac{1}{2}0$ ) in the AFM state (Fig. 4), but not in the FM state (Fig. 5), as also found in recent publications [58–60]. At ambient conditions, FM FeRh is stable but not harmonic, with instabilities nearby (e.g., due to strain) [58]. For the least harmonic phonons, frequency dependence on  $d$  is the strongest. The high-frequency optical phonon modes are harmonic in FM and AFM phases, while the low-frequency acoustic phonons show less harmonic behavior around  $M$ , where the difference between modes, calculated for  $d = 0.04$  and  $0.12$  Å, is the largest (Fig. 4).

Notably, the  $M$ -point phonon instability leads to a cryogenic martensitic transition in AFM FeRh with atomic shuffles of  $d_{Fe} = 0.061$  and  $d_{Rh} = 0.053$  in fractional lattice coordinates, showing that atomic potentials have dimples around the high-temperature symmetric structure (B2) and are inherently anharmonic [61]. One anticipates then a  $d$ -dependence of phonon frequencies, which are well-defined at each fixed  $d$ .

To calculate phonons at a given temperature  $T$ , one could use thermal atomic displacements and forces from *ab initio* molecular dynamics (MD), say, in the ThermoPhonon code [16,104]. A faster, albeit more approximate, method (which we use at  $T_c$  of 353 K) is an application of the quasiharmonic approximation with a finite single-atom displacement  $d$  scaled to a “thermal” potential energy  $E(d) = \frac{1}{2}k_B T$  in an ideal structure (Fig. 6). This method is applied to FeRh in Fig. 5 and shows that AFM B2 structure has an unstable phonon mode at  $M$  with an amplitude of only 0.1  $i$  THz (i.e., close to zero) at “thermal” displacements  $d(T_c) \approx 0.06$  Å [here  $d(Fe) \neq d(Rh)$ , see Fig. 6]; this instability becomes larger at smaller  $d$  (including infinitesimal case used in linear-response methods) and disappears at larger  $d$ .

As phonons in both AFM and FM phases are anharmonic, and the lattice entropy  $S_L$  is affected mostly by the soft phonon modes, this finite-displacement method within a quasiharmonic approximation [105] is a reliable computational “trick” to avoid unstable phonons at a relevant finite temperature; it uses substantially less computational time than the other method based on MD at fixed  $T$  [16], while yielding correct estimates.

The atomic displacement  $d(T)$  can be adjusted to temperature  $T$  (Fig. 6) and used to evaluate the  $T$ -dependent lattice entropy  $S_L[T, d(T)]$ , calculated at fixed lattice constants. Below we use the phonon DOS to evaluate  $\Delta S_L$  at the metamagnetic transition at  $T_c$  (Fig. 7). Importantly, due to anharmonicity and finite thermal displacements at finite temperature,  $\Delta S_L[T_c, d(T_c)]$  is increased by 50%, compared to  $\Delta S_L[T_c, d \rightarrow 0]$ .

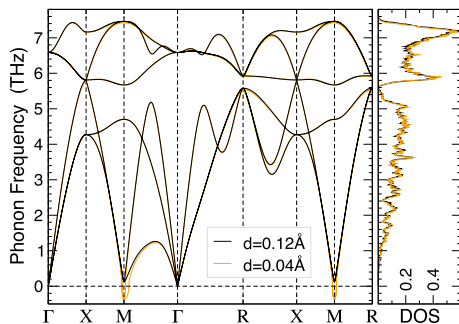


**Figure 4.** (Color online). Phonon frequencies and DOS for AFM B2–FeRh (2.996 Å) using small (0.04 Å) and large (0.12 Å) displacements. Unstable phonons at  $M$  ( $\frac{1}{2}\frac{1}{2}0$ ) appear at  $d \leq 0.06$  Å.

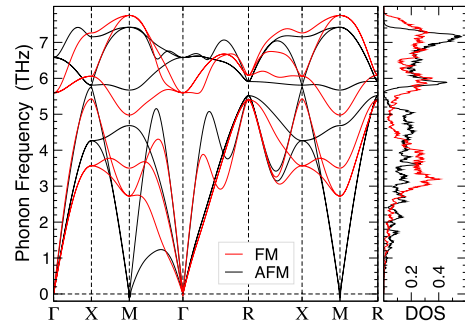


**Figure 5.** (Color online). Phonon frequencies and DOS for FM and AFM states in B2–FeRh (2.996 Å), evaluated with  $d(Fe) \approx d(Rh) \approx 0.06$  Å at  $\frac{1}{2}k_B T_c$ , see text and Fig. 6, now no unstable phonons at  $M$  ( $\frac{1}{2}\frac{1}{2}0$ ).

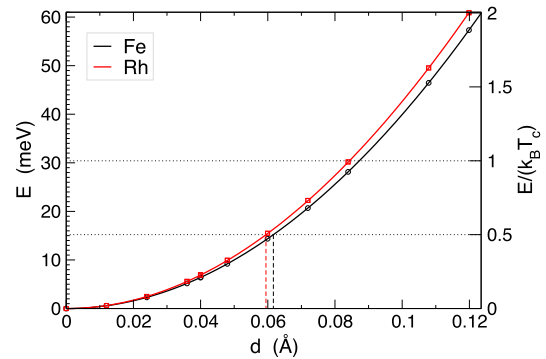


**Figure 6.** (Color online). For FM B2 FeRh (2.997 Å), energy  $E$  (meV) versus displacement  $d$  of a Fe (black) or Rh atom (red) along  $[100]$  compared to  $k_B T_c$ . Lines are quartic fits.

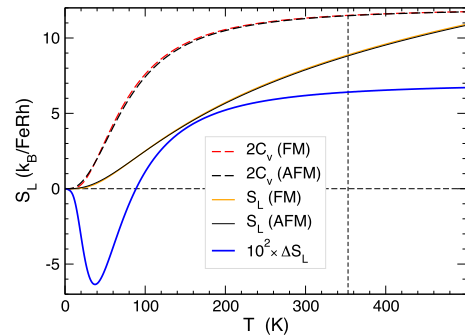


**Figure 7.** (Color online). For B2 FeRh, heat capacity  $C_V$ ,  $S_L$ , and  $\Delta S_L(\text{FM–AFM})$  from phonons (Fig. 5) using  $d(T_c) \approx 0.06$  Å from Fig. 6.  $T_c$  at 353 K is denoted by vertical dashed line.

In particular, for FM B2 FeRh, the energy  $E$  versus atomic displacement  $d$  (shown in Fig. 6) can be fit well by a quartic (not quadratic) polynomial, i.e.,  $E(d) = E^{(2)}d^2 + E^{(4)}d^4$ . We find  $E_{Fe}^{(2)} = 4.003 \text{ eV/Å}^2$  and  $E_{Fe}^{(4)} = -1.030 \text{ eV/Å}^4$  for Fe and  $E_{Rh}^{(2)} = 4.317 \text{ eV/Å}^2$  and  $E_{Rh}^{(4)} = -5.496 \text{ eV/Å}^4$  for Rh. Consequently,  $S_L$  depends on the atomic displacement  $d$ , see Fig. 8. In the FM phase, it changes from  $8.859 k_B/\text{FeRh}$  for small  $d = 0.04$  Å to  $8.972 k_B/\text{FeRh}$  for large  $d = 0.12$  Å at fixed  $a = 2.997$  Å. In the AFM phase, we find a small change from  $8.8176$  to  $8.7945 k_B/\text{FeRh}$  for the same fixed values of  $d$ , see Fig. 8. Interestingly, the unstable AFM B2 phase is less anharmonic than the stable FM B2 phase, which develops phonon instability at a strain [58]. The small- $d$  (0.04 Å) method provides  $\Delta S_L$  of  $0.042 k_B/\text{FeRh}$  (or  $0.02 k_B$  per atom).



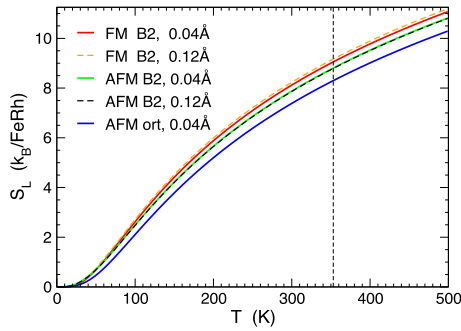


**Figure 8.** (Color online). For B2 and orthorhombic FeRh structures in FM and AFM states at  $P=0$ , lattice entropy  $S_L$  using small (0.04 Å) and large (0.12 Å) atomic displacements  $d$ .

However, with  $T$ -dependent displacements  $d(T_c) \approx 0.06$  Å ( $d_{Fe} \neq d_{Rh}$ , see Fig. 6),  $\Delta S_L[T_c, d(T_c)]$  increases by 50% to  $0.064 k_B/\text{FeRh}$  (or  $0.03 k_B$  per atom), see Fig. 7. Thus, for FeRh, the spin-polarized electrons, fully accounted here, provide the leading contribution to the total entropy change  $\Delta S_T(T_c)$ , while the lattice entropy contribution is smaller (only 28%), but not negligible. This relative contribution agrees with an early prediction [22] and its recent confirmation [53]. Nonetheless, for FeRh,  $\Delta S_L(T_c)$ , now increased by 50% from anharmonicity, is  $\approx 40\%$  of the calculated electronic contribution  $\Delta S_e(T_c) = 0.163 k_B/\text{FeRh}$ .

Anharmonicity affects the phonons and associated thermodynamic quantities. In general, anharmonic effects must be properly included in a consideration of thermodynamics near lattice instabilities and phase transitions. Here, we have described a quick method to include these  $T$ -dependent effects in anharmonic systems by probing the amplitude of atomic displacements  $d$  dependence of the vibrational frequencies. If the phonons were harmonic, then the lattice entropy  $S_L[T, d(T)]$  would not depend on  $d$  [101,105]; Fig. 8 shows that in FeRh this is not the case, as  $d$  in the FM B2 state is larger than for the AFM state.

### 3.5. Entropy change

The total entropy includes the electronic (with magnetic) and lattice contributions. We calculate the total entropy change  $\Delta S = S(\text{FM}) - S(\text{AFM})$  due to electronic transformation at  $T_c = 353$  K at fixed lattice constant  $a = 2.997$  Å (measured [14] in the  $\text{Fe}_{50}\text{Rh}_{50}$  FM phase at  $T_c$ ). We find  $\Delta S_T = 0.227 k_B/\text{FeRh}$ , or  $0.11 k_B/\text{atom}$  (i.e.,  $11.9 \text{ J kg}^{-1} \text{ K}^{-1}$ ) for the isothermal total entropy change at the metamagnetic transformation at  $T_c$  at fixed volume. The lattice entropy contribution  $\Delta S_L$  is 28% of  $\Delta S_T$ ; ignoring the anharmonic effects would lead to a 50% relative error in  $\Delta S_L$  and 14% error in  $\Delta S_T$ .

In experiment, the maximum total entropy change of  $12.5 \pm 1 \text{ J kg}^{-1} \text{ K}^{-1}$  was the same for both baro- and magneto-caloric effects in  $\text{Fe}_{49}\text{Rh}_{51}$  [65]. Three assessment methods gave comparable values for  $\Delta S_T$  for the  $\text{Fe}_{49}\text{Rh}_{51}$  [21], namely, calorimetry:  $12.1$ , Clausius-Clapeyron:  $13.1$ , and Maxwell relations:  $13.6 \text{ J kg}^{-1} \text{ K}^{-1}$ . An earlier measurement [12] yielded  $14.0 \text{ J kg}^{-1} \text{ K}^{-1}$  for stoichiometric FeRh and found a compositional dependence of  $\Delta S$  for the samples doped with Pd, Pt, or Ir. The experimental values [in  $\text{J} \cdot \text{kg}^{-1} \text{ K}^{-1}$ ] for  $\Delta S_T$  of  $13.6$  [21],  $12.5 \pm 1$  [65],  $13 \pm 1$  [85],  $13 \pm 1$  [86], and  $14$  [12] differ from the higher assessed values of  $19 \pm 2$  [30],  $18.3$  [22], and  $17 \pm 3 \text{ J kg}^{-1} \text{ K}^{-1}$  [40]; inaccuracies in Refs. [22,30,40] originated from subtracting values measured at two different compositions [40], using [30]  $\Delta V_P$  instead of  $\Delta V_T$  in the Clausius-Clapeyron equation (7), see section 5, or increasing the extrapolated value of  $(dB_c/dT)_{B=0}$  in eq. (6) to account for an overestimated

magnetocaloric effect in a  $\text{Fe}_{0.48}\text{Rh}_{0.52}$  sample [22]. The assessed values depend on the method [21], sample composition [12], and preparation [19]. The calculated and experimental values are compared in Table 1.

### 3.6. The caloric effect

The maximum isentropic temperature change is

$$\Delta T_S = -T_c \Delta S_T / C_B. \quad (2)$$

Here  $C_B(B, T)$  is the heat capacity at constant magnetic field  $B$ . Using the asymptotic limit  $C_B \approx 3k_B/\text{atom}$  ( $6 k_B/\text{FeRh}$  or  $314 \text{ J kg}^{-1} \text{ K}^{-1}$ ) for solid FeRh at  $T \geq 300$  K (Fig. 7) and our value of  $\Delta S_T$  (section 3.5), we find  $\Delta T_S = -13$  K. This value agrees with the experimental assessments [21], ranging from  $-10.6$  to  $-12$  K, see Table 1. However, it differs from an early estimate [22] of  $\Delta T_S = -(20 \pm 2)$  K, obtained using too high value of  $\Delta S = 18.3 \text{ J kg}^{-1} \text{ K}^{-1}$  in eq. (2). The directly measured adiabatic temperature change  $\Delta T_{ad}(\Delta B)$ , produced by an added external field of  $\Delta B = 1.95$  Tesla, can be as large as  $-12.9$  K for the quenched  $\text{Fe}_{49}\text{Rh}_{51}$  samples [19].

## 4. Estimators for materials screening

### 3.1. Isothermal enthalpy change $\Delta H_T(T_c)$

From Gibbs relation, the isothermal enthalpy change  $\Delta H_T$  at  $T_c$  is the key quantity, given by the formally exact equation

$$\Delta H_T(T_c) = T_c \cdot \Delta S_T(T_c). \quad (3)$$

Using either experimental or calculated (below)  $T_c$  and calculated  $\Delta S_T(T_c) = 11.9 \text{ J kg}^{-1} \text{ K}^{-1}$ , we get  $\Delta H_T(T_c) = 4.2 \text{ kJ/kg}$  or  $6.9 \text{ meV/FeRh}$ . In general,  $\Delta H_T \neq \Delta H_P$ , but  $\Delta H_P$  is typically measured in experiments at fixed external pressure  $P$ .

### 4.2. Transition temperature $T_c$

We note that transition temperature  $T_c$  in eq. (3) can be estimated accurately in mean-field approximations but only if considered separately for segregating (immiscible) [106] and ordering (miscible) systems [107], which have a negative formation enthalpy, e.g., stable solid-solution phase.

For a segregating system, a mean-field approximation was shown to be highly accurate for miscibility gaps (the so-called  $T_0$  line) away from compositional limits (i.e.,  $c_\alpha \rightarrow 0$  or  $c_\alpha \rightarrow 1$  for an  $\alpha$  atomic type), where mean-field entropy differences are less accurate. (Careful Monte Carlo simulations were used to confirm the accuracy [106].) However, in these cases, vibrational entropy changes can have a large effect in  $T_c$ , where analytically it is changed when going between two phases (e.g., solid solution and segregation) as

$$T_c = T_{c, \text{conf}} \left( 1 + \frac{\Delta S_L}{\Delta S_{\text{conf}}} \right)^{-1}, \quad (4)$$

where the subscript “conf” delineates the configurational entropy only and  $\Delta S_L$  is the lattice vibrations entropy changes. Moreover, to a good approximation (at least in binary metals) [108,109], the lattice vibrational change  $\Delta S_L \approx -0.34 \Delta \chi$ , where  $\Delta \chi$  is the electronegativity difference between alloying pairs. So, if the electronegativities of elemental pairs are similar, there is no effect from vibrations on  $T_c$  and estimates without vibrational calculations are fine, as discussed in Ref. [106]. Otherwise, changes in vibrational

entropy can be estimated at a given temperature, as we have outlined earlier.

Typically, the sign of a formation enthalpy  $H_f$  indicates either segregation ( $H_f > 0$ ) or ordering ( $H_f \leq 0$ ) tendency. Any diffusion broadens the hysteresis, while a chemical inhomogeneity smears a diffusionless phase transition; both effects are consequences of a segregation tendency, which should be avoided in caloric materials. Fortunately, a positive formation enthalpy can easily be monitored during materials screening.

In contrast to segregation, for immiscible alloys  $T_c$  for a first-order transition between two phases (e.g., FM and AFM FeRh exemplified here) can be estimated well by

$$T_c = I_c \cdot \delta H_0 / k_B, \quad (5)$$

where  $\delta H_0$  is the enthalpy difference between fully-relaxed structures at zero temperature, and  $I_c \sim 1$  (dimensionless) is a factor with a constant value for a class of similar systems. Please keep in mind that  $\delta H_0$  should not be confused with  $\Delta H_T(T_c)$ , and, as expected,  $\Delta H_T(T_c) \ll \delta H_0(0 \text{ K})$ , as numerically exemplified before [110]. We have found that eq. (5) accurately estimates order-disorder transitions in metallic alloys [111,112] and martensitic phase transitions [16,17,107].

Equation (5) with  $I_c = 1$  is exact for barrierless transitions, whereas generally  $I_c$  is proportional to a ratio (of functions of order parameters) nearing 1 between the two systems, such as two magnetic configurations in a fixed chemical cell or in an order-disorder transitions in a fixed magnetic state [107]. For example, the calculated enthalpy difference  $\delta H_0$  between AFM and FM B2–FeRh is  $29.8 \pm 1$  meV/atom (Fig. 3); this value compares well with previous calculations [49]. For the metamagnetic phase transition in FeRh, we find that  $(\delta H_0/k_B) = 346 \pm 12$  K, which compares well with  $T_c = 353 \pm 1$  K measured in Fe<sub>50</sub>Rh<sub>50</sub> [29]. The value of  $I_c$  near 1 has uncertainty due to an error in DFT energies and in the measured  $T_c$ . As the chemical structure is fixed for FeRh metamagnetic transition and only the magnetic configuration changed, it is purely an electronic configurational change.

Equations (3) and (5) are exact, while  $I_c \approx 1$  is approximate. For barrierless transitions, the enthalpy difference  $\delta H_0$  coincides with the energy needed to excite an additional degree of freedom (DoF) and access the higher-temperature phase, and in the classical limit  $I_c \equiv 1$  in this case. This interpretation of eq. (5) was successfully applied to estimate melting temperatures [113]. The apparent simplicity of the estimate (5) obscures a complicated counting of the number of the effective DoF [113]. In general, a higher- $T$  phase has more DoF contributing and consequently a higher entropy than the lower- $T$  phase. The change in the number of effective DoF is an integer, hence, a reasonable accuracy of eq. (5) with  $I_c \approx 1$  is not a coincidence. As both atomic and spin orderings can be described by a basis-set expansion [97], a similar equation for different physics is obtained. One can assess eq. (5) for generic alloy screening, as exemplified for order-disorder transitions in Table 2 or for solid-solid phase transitions in Table 3.

#### 4.3. Compositional sensitivity of $T_c$

Notably,  $T_c$  scales with  $\delta H_0$  in both stoichiometric (50 at.% Rh) and off-stoichiometric alloys with a partial atomic disorder, including with long-range order parameter, see, e.g., Ref. [107]. From the electronic density of states (DOS)  $n(E)$  in Fig. 2, also seen in recent calculations [57–59], we expect that lowering of the Fermi energy  $E_F$  (due to decrease in Rh fraction) will stabilize the FM phase (from a lower DOS in the pseudogap), but it would have a lesser effect on the AFM phase. This change will decrease  $\delta H_0$  and will reduce  $T_c$ . Indeed, this qualitative expectation agrees with the

**Table 2**

Calculated order-disorder enthalpies  $\delta H_0$  (meV/atom) and  $k_B T_c$  (meV) and  $T_c$  (K) for some fcc (miscible) binaries, using our data from Table 3.4 in Ref. [110]. Strukturbericht designations in brackets [...] are assumed ground states; structures in parenthesis (...) are metastable. Calculated  $T_c$ 's were obtained from Monte Carlo using a cluster expansion, and compared to experimental (Expt.) values [120,121].

System	GS	$\delta H_0$ (meV)	$k_B T_c$ (meV)	$T_c$ (K)	Expt. (K)	$I_c^{-1}$	Ref.
Ag <sub>3</sub> Al	(D0 <sub>22</sub> )	46	45	520	—	0.98	[114–116]
Ag <sub>2</sub> Al	(MoPt <sub>2</sub> )	41	37	430	—	0.91	[114–116]
AgAu	[L1 <sub>0</sub> ]	12.2	14	165	—	1.13	[117]
AgAu	[L1 <sub>0</sub> ]	16.7	—	—	—	—	[118]
CuAu	L1 <sub>0</sub>	47	48.3	560	658	1.03	[119]
Cu <sub>3</sub> Au	[L1 <sub>2</sub> ]	42.8	—	—	500	—	[118]
Ni <sub>3</sub> V	D0 <sub>22</sub>	115	118	1370	1318	1.03	[97]

**Table 3**

Calculated examples of relative enthalpies  $\delta H_0$  (meV/atom) between low- $T$  and high- $T$  phases are compared to experimental  $T_c$ 's [121,123], with  $I_c^{-1} = \delta H_0/k_B T_c$  (dimensionless).

System	Phase	Transition	$\delta H_0$ (meV)	$\delta H_0/k_B$ (K)	$T_c$ (K)	$I_c^{-1}$	Ref.
Ti	hcp	hcp-bcc	97.2	1128	1155	0.976	present
Hf	hcp	hcp-bcc	174.2	2022	2016	1.003	present
NiTi	bco	martensitic	29.5	343	333	1.030	[17]
FePd	L1 <sub>0</sub>	FM-PM	64.5	749	730	1.026	[122]
FePt	L1 <sub>0</sub>	FM-PM	63.3	735	750	0.980	[122]
CoPt	L1 <sub>0</sub>	FM-PM	59.6	692	720	0.961	[122]
MnNiSi	<i>Pnma</i>	FM-PM	55.7	646	662	0.976	present
LiBH <sub>4</sub>	<i>Pnma</i>	melting	45.3	526	553	0.951	[123]
FeRh	B2	AFM-FM	29.8	346	353	0.980	present

experimental phase diagram [29,37,124]. Compositional hypersensitivity of FeRh was theoretically studied in Ref. [53].

#### 4.4. Field dependence of $T_c$

Dependence of  $T_c$  on the external magnetic field  $B$ , as well as dependence of the critical field  $B_c$  on  $T$ , assuming  $(dB_c/dT)^{-1} = dT_c/dB$ , can be determined from discontinuities in magnetization  $M$  and entropy  $S$  at the first-order metamagnetic transition:

$$\frac{dT_c}{dB} = \frac{\Delta M_{T=T_c}}{\Delta S_{T=T_c}}. \quad (6)$$

The calculated magnetizations of the fully-relaxed B2–FeRh in AFM and FM states are 0 and  $2.1 \mu_B/\text{atom}$ , respectively (Section 3.1). For the upper bound  $\Delta M(T_c) < [M(\text{FM}) - M(\text{AFM})]$  for the magnetization change at  $T_c$ , we find  $\Delta M/\Delta S_T < 2.1 \mu_B/0.103 k_B = 13.7$  K/Tesla. However, a more realistic value [42] of  $(\Delta M)_{T_c} - 60\%$  of the upper bound – gives  $-dT_c/dB = 8.2$  K/Tesla for stoichiometric FeRh. Measurements of  $T_c(B)$  in the external magnetic field (or critical field vs.  $T$ ) provide a quadratic [34] dependence with the linear [30] slope  $-dT_c/dB$  in small fields of 8.2 in FeRh [12]; 8.2 in Fe<sub>49.5</sub>Rh<sub>50.5</sub> [42]; 8.5 in Fe<sub>49</sub>Rh<sub>51</sub> [21]; and from 9.6 to 9.7 K/Tesla in Fe<sub>49</sub>Rh<sub>51</sub> [65].

#### 4.5. Accuracy

As shown, a number of standard approximations within DFT calculations work very well for estimating many thermodynamic quantities, in particular for caloric properties, such as transition temperatures  $T_c$ , field-dependent changes in  $T_c$ , and electronic entropy changes  $\Delta S_e$  (the main contribution), while the significant lattice entropy changes  $\Delta S_L$  are underestimated for anharmonic

atomic vibrations, which are found in many systems with lattice instabilities. However, we established a direct method to evaluate more correctly  $\Delta S_L$ , which gave a 50% increase in its magnitude, and provided more accurate estimates of caloric properties, see Table 1. It remains to test these estimators in more complex systems to screen for improved caloric materials via an approach presented recently (8).

## 5. Issues with indirect assessments

Before closing, we would be remiss not to remark on quantities that are difficult to assess theoretically due to errors or inability to measure experimentally, clearly relevant to materials screening, and occasional incorrectly applied.

Often the measured  $dT_c/dP$  and  $\Delta V$  is used to evaluate  $\Delta S$  using the Clausius-Clapeyron equation

$$\frac{dT_c}{dP} = \frac{\Delta V_T}{\Delta S_P} \quad (7)$$

However, there is a well-known problem with applications of this equation to experimental data [125]. Specifically, while it is possible to measure pressure  $P$  and the corresponding volume change ( $\Delta V_P$ ) at a first-order transition, the isothermal volume change ( $\Delta V_T$ ) induced by varying  $P$  is not measured; and, furthermore, there is no reason that  $\Delta V_T$  and  $\Delta V_P$  are the same. Nonetheless, there have been instances where  $\Delta V_P$  was used as equal to  $\Delta V_T$  to use eq. (7), which gives an overestimate of  $\Delta S$ , see, for example, Ref. [30]. Such disagreements of estimates from eq. (7) and direct measurements are well documented [125]. Pressure dependence of  $T_c$  has been long discussed [30,125,126]; the measurements [126] of  $dT_c/dP$  in FeRh range from 43 [30] to 64 K/GPa [65].

Regarding the accuracy of DFT-calculated energy ( $E$ ) versus volume ( $V$ ) curves (Fig. 3), the lattice constants  $a_0$  (at  $P = 0$  GPa,  $T = 0$  K) are 2.996 Å in AFM and 3.012 Å in FM phase for B2 FeRh, while the measurements on Fe<sub>50</sub>Rh<sub>50</sub> at 353K give 2.987 Å and 2.997 Å [14], similar to results in Ref. [30], see our Table 1. So, with calculated lattice constants having a relative error of  $\pm 0.3\%$ , the calculated volume  $V \sim a^3$  has an error of  $\pm 1.2\%$ , too large to determine reliably a change of  $\Delta V/V \approx 1\%$ , as found relevant in experiment [14]. So, one cannot use the Clausius-Clapeyron relation to assess  $dT_c/dP$ , if looking for outliers for desired caloric properties.

Magnetic entropy  $S_M$  is typically assessed by thermodynamic integration using experimental data:

$$\Delta S_M(T, \Delta H) = \int_{H_1}^{H_2} dH \frac{\partial M(T, H)}{\partial T} \Big|_H \quad (8)$$

Importantly, this equation is valid within a single phase. Derivative  $\partial M/\partial T$  diverges at the metamagnetic first-order phase transition. Thermodynamic integration should not be performed across phase boundaries.

In addition, the difference between values in two phases should be calculated by subtracting values obtained for the same chemical composition, otherwise improper or misleading results can be derived, as in Ref. [40], where two epitaxial Fe–Rh films of different compositions we used, i.e., Fe-rich with FM ground state and Rh-rich with AFM ground state.

## 6. Generic remarks

### 6.1. Bounds and dominant contributions for entropy change

For any type of screening, it is useful to note the largest

contributions that can be expected to control desired behavior. For caloric behavior, electronic and lattice entropy changes due to electronic- or structural-driven instabilities are most critical and we can approximate the largest possible values. Namely, for  $d$ -band ( $f$ -band) systems, the electronic spin (magnetic) entropy changes  $\Delta S_e \leq \Delta S_e^{max}$  have upper limit of  $\Delta S_e^{max}/k_B = \ln(2^{n/2})$  of 3.47 (4.85) per half-filled band with  $n$  being 10  $d$  (14  $f$ ) orbitals; this is essentially the maximum permitted magnetic entropy change from atomic magnetization.  $\Delta S_e$  cannot be larger than the electronic entropy  $S_e$  of either phase, as estimated by eq. (1). A phase transition accompanied by a large change of electrical conductivity (proportional to electronic DOS at  $E_F$ , i.e.,  $n(E_F)$ ) is expected to have a good  $\Delta S_e$ .

If the transition temperature between competing states is above the respective Debye temperatures, the vibrational entropy change for a solid-solid transition is approximated by

$$\Delta S_L \approx 3k_B \ln(\Theta_2^D/\Theta_1^D), \quad (9)$$

where  $\Theta_\alpha^D$  is the Debye temperature of the phase  $\alpha$ . For  $\Theta_2^D/\Theta_1^D$  of 1.0–1.5, a safe upper-bound range for solids of the same stoichiometry and pressure, we get  $0 \leq \Delta S_L < 1.22 k_B/\text{atom}$  for quasi-harmonic solids, a bound smaller than that for electronic contributions (i.e.,  $\Delta S_L < \Delta S_e$ ). Also,  $\Delta S_L$  in a solid with non-harmonic phonons can be larger than that in a harmonic solid, as already demonstrated. The general expectation then is that the combined electronic and magnetic entropy changes will constitute the dominant contributions to the total  $\Delta S_T$  for caloric systems, while the lattice entropy can be significant but secondary (and more demanding to estimate reliably). An estimate of the dominant effect (and its bounds) is used for the high-throughput pre-screening of materials [8,81].

### 6.2. Chemical disorder and segregation

Caloric material is expected to have a phase transition at the target temperature  $T$ . However, stoichiometric line compounds typically have off-target values of  $T_c$ . To correct this, chemical composition is altered and an off-stoichiometric chemical disorder is introduced. For a large caloric effect, the first-order phase transition must be sharp, and consequently the caloric material must be chemically homogeneous. Any segregation will be detrimental to such homogeneity.

To screen out segregating materials, we use the coherent-potential approximation (CPA) [95], implemented in the KKR electronic-structure code [96], to compute dependences of the formation enthalpy  $H_f$  on composition  $c$ , considering possible disorder on each sublattice. (One can also use large representative supercells at a number of discrete compositions, but, if done carefully, those results usually compare well with the output of KKR-CPA, which is much faster to compute due to smaller cells with fewer atoms and electrons.) If immiscible, i.e.,  $\partial^2 H_f/\partial c^2 < 0$ , then  $H_f(c)$  is concave and the system can lower its energy by developing a compositional inhomogeneity (segregation) that is unfavorable for calorics. Such materials are rejected, such as (Hf<sub>1-c</sub>Nb<sub>c</sub>)Fe<sub>2</sub> Lave's phase (Fig. 9 in Ref. [127]). In contrast, a convex  $H_f(c)$  (in miscible system with  $\partial^2 H_f/\partial c^2 > 0$ ) is a necessary but not sufficient condition for good caloric properties. An example with a convex  $H_f(c)$  is ZrMn<sub>6</sub>(Sn<sub>1-c</sub>Sb<sub>c</sub>), see Fig. 8 in Ref. [8].

### 6.3. Hysteresis

A first-order phase transition is usually accompanied by a hysteresis. The width of the hysteresis serves as huge loss factor for



caloric cooling, unless the hysteresis can be eliminated [128]. Nucleation, lattice mismatch, and enthalpy barriers for nucleation and phase boundary propagation contribute to the width of the hysteresis. Fortunately, we know how to reduce the hysteresis width.

Compositional changes affects the lattice constants in each phase. The lattice mismatch between austenite and martensite can be made to go to zero and the hysteresis thereby narrowed by the fine tuning of composition  $c$  [129], which occurs when the middle eigenvalue ( $\lambda_2$ ) of the transformation stretch tensor attains the value 1 at  $T_c$ . While  $\lambda_2(c)$  could be monitored versus composition, it is far more convenient and straightforward to assess the dependence of the lattice constants in the relevant phases on composition at fixed  $(P, T)$ , as computed in DFT, see section 2. The KKR-CPA permits to do this easily and quickly for materials with disorder, as we have done many times. Typically, only a few calculations are needed to find compositions where lattice match is achieved.

Finally, defects (e.g., surface geometry, bulk impurities, precipitates, or second-phase remnants due to incomplete transformation) can serve as nucleation centers, suppressing the nucleation enthalpy barriers. Design of caloric devices should account for the nucleation centers in caloric materials. The enthalpy barriers for the phase boundary propagation depend on composition. We calculate them using the nudged elastic band (NEB) methods [98,100,130]. Unfortunately,  $T_c$  depends on composition, too. Hence, reduction of the hysteresis at constant  $T_c$  by adjusting  $c$  is similar to tuning a piano: several compositional degrees of freedom must be simultaneously or iteratively adjusted to get the target values for both  $T_c$  and hysteresis width. Nevertheless, trends can be assessed with relatively few calculations to find better design regions, or eliminate systems quickly [8].

## 7. Beyond FeRh: novel materials with giant magnetocaloric response

Recently, we utilized some of these methods to search among 10,000+ candidates and to reduce systems of interest for our experimental collaborators, eliminating thousands alloys [8]. Out of all systems scanned, about ten (or 0.1%) were found (“predicted”) to have caloric behavior either similar to FeRh (i.e.,  $\Delta S_T \geq 12 \text{ J kg}^{-1} \text{ K}^{-1}$ ), but lower in cost or significantly improvable with modifications to alloying chemistry. Several classes of these materials are now being investigated experimentally. For example, Ni-Co-Mn-Ti [131] and  $\text{Mn}_{0.5}\text{Fe}_{0.5}\text{NiSi}_{1-x}\text{Al}_x$  [132] have been confirmed to be promising for the solid-state refrigeration, with enhancement of  $\Delta S_T$  well above  $20 \text{ J kg}^{-1} \text{ K}^{-1}$  at room temperature. Such discovery will be accelerated when this type of screening is implemented through a database combined with key correlations derived by machine-learning techniques, especially when looking for outliers in desired properties – just as with systems with zero hysteresis at phase transformations, where the desired compositional range may consist of a single point [129].

## 8. Summary

We have explored several thermodynamic estimates for assessing caloric properties in alloys. We used FeRh as a testbed, as it exhibits large multicaloric (magneto-, elasto- and baro-caloric) responses at its metamagnetic transition just above room temperature, as well as non-harmonic vibrations – typical for systems near lattice instabilities. We showed that use of controlled  $T$ -dependent atomic displacements, easily estimated at  $T_c$ , provides a reliable assessment of lattice entropy changes at the phase transition. In FeRh, we tested approximate methods and estimators, and evaluated a number of thermodynamic properties, including

specific heat, entropy and enthalpy changes, transition temperature, and isentropic temperature drop. The predicted caloric properties are in a quantitative agreement with the trusted experimental data, see Table 1. We have verified that these estimators are reliable (if applied carefully) and accurate. In contrast, we showed that some previously used assessments, like from the Clausius-Clapeyron relation (7), are unreliable due to the underlying assumptions. Thus, assessment and testing of the methods were a necessity.

Tested reliable methods will enable faster theory-guided screening to find more promising caloric materials, involving more complex multicomponent systems on which to focus. Indeed, the estimates provided here already resulted in finding improved lower-cost caloric systems exhibiting giant magnetocaloric enhancements with promise for use in solid-state cooling [131,132].

## Acknowledgments

We thank Dr. Vitalij Pecharsky and Dr. Klaus Ruedenberg for discussions. Our theory developments at Ames Laboratory and Iowa State University were funded by the U.S. Department of Energy, Office of Science, Basic Energy Sciences, Materials Science and Engineering Division. Ames Laboratory is operated for the U.S. DOE by Iowa State University under contract DE-AC02-07CH11358. Initial application to caloric materials discovery coupled with experimental studies was partly supported by the U.S. DOE, Advanced Manufacturing Office of the Office of Energy Efficiency and Renewable Energy through CaloriCool™ – the Caloric Materials Consortium established as a part of the U.S. DOE Energy Materials Network [133].

## References

- [1] V.K. Pecharsky, J. Cui, D.D. Johnson, (magneto)caloric refrigeration: is there light at the end of the tunnel? *Phil. Trans. R. Soc. A* 374 (2016) 20150305, <https://doi.org/10.1098/rsta.2015.0305>. <http://rsta.royalsocietypublishing.org/content/374/2074/20150305>.
- [2] O. Gutfleisch, M.A. Willard, E. Brück, C.H. Chen, S.G. Sankar, J.P. Liu, Magnetic materials and devices for the 21st century: stronger, lighter, and more energy efficient, *Adv. Mater.* 23 (7) (2011) 821–842, <https://doi.org/10.1002/adma.201002180>.
- [3] K. Gschneidner, V. Pecharsky, Thirty years of near room temperature magnetic cooling: where we are today and future prospects, *Int. J. Refrig.* 31 (6) (2008) 945–961, <https://doi.org/10.1016/j.ijrefrig.2008.01.004>. <http://www.sciencedirect.com/science/article/pii/S0140700708000236>.
- [4] A.F. Ioffe, A.V. Ioffe, Certain regularities in the magnitude of the thermal conductivity of semiconductors, *Dokl. Akad. Nauk SSSR* 97 (1954) 821.
- [5] W.F. Giaque, A thermodynamic treatment of certain magnetic effects, a proposed method of producing temperatures considerably below 1k absolute, *J. Am. Chem. Soc.* 49 (1927) 1864–1870.
- [6] P. Debye, Einige bemerkungen zur magnetisierung bei tiefer temperatur, *Ann. Phys.* 386 (1926) 1154–1160.
- [7] M.A. Cazin, Memoire sur les effets thermiques du magnetisme, *Ann. Chem. Phys.* 6 (1875) 493–554.
- [8] N.A. Zarkevich, D.D. Johnson, V.K. Pecharsky, High-throughput search for caloric materials: the caloricoool approach, *J. Phys. D Appl. Phys.* 51 (2) (2017) 024002, <https://doi.org/10.1088/1361-6463/aa9bd0>. <http://stacks.iop.org/0022-3727/51/i=2/a=024002>.
- [9] L. Manosa, A. Planes, Special issue on caloric materials, *J. Phys. D Appl. Phys.* 51 (7) (2018) 070201, <https://doi.org/10.1088/1361-6463/aaa7c4>. <http://stacks.iop.org/0022-3727/51/i=7/a=070201>.
- [10] L. Muldrew, F. deBergevin, Antiferromagnetic-ferromagnetic transformation in FeRh, *J. Chem. Phys.* 35 (5) (1961) 1904–1905, <https://doi.org/10.1063/1.1732175>. <https://doi.org/10.1063/1.1732175>.
- [11] E.P. Abrahamson, S.L. Lopata, The lattice parameters and solubility limits of alpha-iron as affected by some binary transition-element additions, *Transactions of the Metallurgical Society of AIME* 236 (1966) 76–87.
- [12] J.S. Kouvel, Unusual nature of the abrupt magnetic transition in FeRh and its pseudobinary variants, *J. Appl. Phys.* 37 (1966) 1257, <https://doi.org/10.1063/1.1708424>. <https://aip.scitation.org/doi/10.1063/1.1708424>.
- [13] J.M. Lommel, J.S. Kouvel, Effects of mechanical and thermal treatment on the structure and magnetic transitions in FeRh, *J. Appl. Phys.* 38 (3) (1967) 1263–1264, <https://doi.org/10.1063/1.1709570>. <https://doi.org/10.1063/1.1709570>.
- [14] L. Zsoldos, Lattice parameter change of FeRh alloys due to antiferromagnetic-



- ferromagnetic transformation, *Phys. Status Solidi* 20 (1) (1967) K25–K28, <https://doi.org/10.1002/pssb.19670200148>. <https://doi.org/10.1002/pssb.19670200148>.
- [15] W.J. Buehler, J.V. Gilfrich, R.C. Wiley, Effect of low-temperature phase changes on the mechanical properties of alloys near composition *tini*, *J. Appl. Phys.* 34 (5) (1963) 1475–1477, <https://doi.org/10.1063/1.1729603>. <https://doi.org/10.1063/1.1729603>.
- [16] N.A. Zarkevich, D.D. Johnson, Stable atomic structure of NiTi austenite, *Phys. Rev. B* 90 (2014) 060102, <https://doi.org/10.1103/PhysRevB.90.060102>. <https://doi.org/10.1103/PhysRevB.90.060102>.
- [17] N.A. Zarkevich, D.D. Johnson, Shape-memory transformations of NiTi: minimum-energy pathways between austenite, martensites, and kinetically limited intermediate states, *Phys. Rev. Lett.* 113 (2014) 265701, <https://doi.org/10.1103/PhysRevLett.113.265701>. <https://link.aps.org/doi/10.1103/PhysRevLett.113.265701>.
- [18] J. Cui, Y. Wu, J. Muehlbauer, Y. Hwang, R. Radermacher, S. Fackler, M. Wuttig, I. Takeuchi, Demonstration of high efficiency elastocaloric cooling with large  $\delta T$  using NiTi wires, *Appl. Phys. Lett.* 101 (7) (2012) 073904, <https://doi.org/10.1063/1.4746257>. <https://aip.scitation.org/doi/10.1063/1.4746257>.
- [19] S. Nikitin, G. Myalikgulyev, A. Tishin, M. Annaorazov, K. Asatryan, A. Tyurin, The magnetocaloric effect in Fe<sub>49</sub>Rh<sub>51</sub> compound, *Phys. Lett.* 148 (6–7) (1990) 363–366, [https://doi.org/10.1016/0375-9601\(90\)90819-A](https://doi.org/10.1016/0375-9601(90)90819-A). <http://www.sciencedirect.com/science/article/pii/037596019090819A>.
- [20] M.P. Annaorazov, S.A. Nikitin, A.L. Tyurin, K.A. Asatryan, A.K. Dovletov, Anomalous high entropy change in FeRh alloy, *J. Appl. Phys.* 79 (3) (1996) 1689–1695, <https://doi.org/10.1063/1.360955>. <https://doi.org/10.1063/1.360955>.
- [21] A. Chirkova, K. Skokov, L. Schultz, N. Baranov, O. Gutfleisch, T. Woodcock, Giant adiabatic temperature change in FeRh alloys evidenced by direct measurements under cyclic conditions, *Acta Mater.* 106 (2016) 15–21, <https://doi.org/10.1016/j.actamat.2015.11.054>. <https://www.sciencedirect.com/science/article/pii/S1359645415301051>.
- [22] B.K. Ponomarev, Investigation of the antiferro-ferromagnetism transition in an FeRh alloy in a pulsed magnetic field up to 300 koe, *Soviet Physics JETP* 36 (1973) 105, translated from *Zh. Eksp. Teor. Fiz.* 63 (1972) 199–204. <http://www.jetp.ac.ru/cgi-bin/e/index/e/36/1/p105?a=list>.
- [23] M. Pugacheva, J. Morkowski, A. Jezierski, A. Szajek, On a structural phase transition in the ordered FeRh alloy, *Solid State Commun.* 92 (9) (1994) 731–734, [https://doi.org/10.1016/0038-1098\(94\)90762-5](https://doi.org/10.1016/0038-1098(94)90762-5). <http://www.sciencedirect.com/science/article/pii/0038109894907625>.
- [24] M.R. Ibarra, P.A. Algarabel, Giant volume magnetostriction in the FeRh alloy, *Phys. Rev. B* 50 (1994) 4196–4199, <https://doi.org/10.1103/PhysRevB.50.4196>. <http://link.aps.org/doi/10.1103/PhysRevB.50.4196>.
- [25] M. Fallot, Les alliages du fer avec les métaux de la famille du platine, *Ann. Phys.* 10 (1938) 291–332.
- [26] M. Fallot, R. Hocart, Sur l'apparition du ferromagnétisme par élévation de température dans des alliages de fer et de rhodium, *Rev. Sci.* 77 (1939) 498.
- [27] F. de Bergevin, L. Muldower, Etude cristallographique de certains alliages ferrhodium, *Compt. Rend.* 252 (1961) 1347, <https://gallica.bnf.fr/ark:/12148/bpt6k32049/f1387.image>.
- [28] J.S. Kouvel, C.C. Hartelius, Anomalous magnetic moments and transformations in the ordered alloy FeRh, *J. Appl. Phys.* 33 (3) (1962) 1343, <https://doi.org/10.1063/1.1728721>. <https://doi.org/10.1063/1.1728721>.
- [29] G. Shirane, C.W. Chen, P.A. Flinn, R. Nathans, Mössbauer study of hyperfine fields and isomer shifts in the Fe-Rh alloys, *Phys. Rev.* 131 (1963) 183–190, <https://doi.org/10.1103/PhysRev.131.183>. <http://link.aps.org/doi/10.1103/PhysRev.131.183>.
- [30] A.I. Zakharov, A.M. Kadomtseva, R.Z. Levitin, E.G. Ponyatovskii, Magnetic and magnetoelastic properties of a metamagnetic iron-rhodium alloy, *Soviet Physics JETP* 19 (1964) 1348, translated from: *Zh. Eksp. Teor. Fiz.* 46 (6) (1964) 2003–2010. <http://www.jetp.ac.ru/cgi-bin/e/index/e/19/6/p1348?a=list>.
- [31] G. Shirane, R. Nathans, C.W. Chen, Magnetic moments and unpaired spin densities in the Fe-Rh alloys, *Phys. Rev.* 134 (1964) A1547–A1553, <https://doi.org/10.1103/PhysRev.134.A1547>. <http://link.aps.org/doi/10.1103/PhysRev.134.A1547>.
- [32] H.L. Walter, Exchange inversion in ternary modifications of iron rhodium, *J. Appl. Phys.* 35 (3) (1964) 938–939, <https://doi.org/10.1063/1.1713547>.
- [33] R.Z. Levitin, B.K. Ponomarev, Magnetostriction of the metamagnetic iron-rhodium alloy, *Soviet Physics JETP* 23 (1966) 984, translated from: *Zh. Eksp. Teor. Fiz.* 50 (1966) 1478–1480. <http://www.jetp.ac.ru/cgi-bin/e/index/e/23/6/p984?a=list>.
- [34] J.B. McKinnon, D. Melville, E.W. Lee, The antiferromagnetic-ferromagnetic transition in iron-rhodium alloys, *J. Phys. Chem.* 3 (15) (1970) S46, <https://doi.org/10.1088/0022-3719/3/15/306>. <http://stacks.iop.org/0022-3719/3/i=15/a=306>.
- [35] L. Vinokurova, A. Vlasov, N. Kulikov, M. Pardavi-Horváth, Pressure-induced antiferromagnetism in ferromagnetic Fe<sub>51</sub>Rh<sub>48.5</sub> alloy, *J. Magn. Magn. Mater.* 25 (2) (1981) 201–206, [https://doi.org/10.1016/0304-8853\(81\)90120-7](https://doi.org/10.1016/0304-8853(81)90120-7). <http://www.sciencedirect.com/science/article/pii/0304885381901207>.
- [36] M. Annaorazov, K. Asatryan, G. Myalikgulyev, S. Nikitin, A. Tishin, A. Tyurin, Alloys of the Fe-Rh system as a new class of working material for magnetic refrigerators, *Cryogenics* 32 (10) (1992) 867–872, [https://doi.org/10.1016/0011-2275\(92\)90352-B](https://doi.org/10.1016/0011-2275(92)90352-B). <http://www.sciencedirect.com/science/article/pii/001122759290352B>.
- [37] J. Balun, L. Eleno, G. Inden, Phase equilibria in the Fe-Rh-Ti system i. experimental results, *Intermetallics* 15 (9) (2007) 1237–1247, <https://doi.org/10.1016/j.intermet.2007.03.002>. <http://www.sciencedirect.com/science/article/pii/S0966979507000507>.
- [38] S. Inoue, H. Yu Yu Ko, T. Suzuki, Magnetic properties of single-crystalline FeRh alloy thin films, *IEEE Trans. Magn.* 44 (2008) 2875, <https://doi.org/10.1109/TMAG.2008.2001846>.
- [39] I. Radu, C. Stamm, N. Pontius, T. Kachel, P. Ramm, J.-U. Thiele, H.A. Dürr, C.H. Back, Laser-induced generation and quenching of magnetization on FeRh studied with time-resolved x-ray magnetic circular dichroism, *Phys. Rev. B* 81 (2010) 104415, <https://doi.org/10.1103/PhysRevB.81.104415>. <http://link.aps.org/doi/10.1103/PhysRevB.81.104415>.
- [40] D.W. Cooke, F. Hellman, C. Baldasseroni, C. Bordel, S. Moyerman, E.E. Fullerton, Thermodynamic measurements of Fe-Rh alloys, *Phys. Rev. Lett.* 109 (2012) 255901, <https://doi.org/10.1103/PhysRevLett.109.255901>. <http://link.aps.org/doi/10.1103/PhysRevLett.109.255901>.
- [41] Y. Wakasaka, Y. Uemura, T. Yokoyama, H. Asakura, H. Morimoto, M. Tabuchi, D. Ohshima, T. Kato, S. Iwata, Anomalous structural behavior in the metamagnetic transition of FeRh thin films from a local viewpoint, *Phys. Rev. B* 92 (2015) 184408, <https://doi.org/10.1103/PhysRevB.92.184408>. <http://link.aps.org/doi/10.1103/PhysRevB.92.184408>.
- [42] R. Onodera, K. Ohtake, K. Takahashi, S. Kimura, K. Watanabe, K. Koyama, Observation of a metamagnetic transition of FeRh alloy under high magnetic fields and high temperatures, *Journal of the Japan Institute of Metals and Materials* 80 (3) (2016) 186–191, <https://doi.org/10.2320/jinstmet.2015055>.
- [43] F. Pressacco, V. Uhlir, M. Gatti, A. Bendounan, E.E. Fullerton, F. Sirotti, Stable room-temperature ferromagnetic phase at the FeRh(100) surface, *Sci. Rep.* 6 (2016) 22383, <https://doi.org/10.1038/srep22383>.
- [44] M.G. Loving, R. Barua, C.L. Graët, C.J. Kinane, D. Heiman, S. Langridge, C.H. Marrows, L.H. Lewis, Strain-tuning of the magnetocaloric transition temperature in model FeRh films, *J. Phys. D Appl. Phys.* 51 (2018) 024003, <https://doi.org/10.1088/1361-6463/aa9d1f>. <http://iopscience.iop.org/article/10.1088/1361-6463/aa9d1f>.
- [45] D.J. Keavney, Y. Choi, M.V. Holt, V. Uhlir, D. Arena, E.E. Fullerton, P.J. Ryan, J.-W. Kim, Phase coexistence and kinetic arrest in the magnetostructural transition of the ordered alloy FeRh, *Sci. Rep.* 8 (1) (2018) 1778, <https://doi.org/10.1038/s41598-018-20101-0>. <https://doi.org/10.1038/s41598-018-20101-0>.
- [46] V.I. Zverev, A.P. Pyatakov, A.A. Shtil, A.M. Tishin, Novel applications of magnetic materials and technologies for medicine, *J. Magn. Magn. Mater.* 459 (2018) 182–186, <https://doi.org/10.1016/j.jmmm.2017.11.032>. <http://WOS:000432615700035>.
- [47] N.P. Grazhdankina, Magnetic first order transitions, *Sov. Phys. Usp.* 11 (1969) 727–745.
- [48] H. Hasegawa, Electronic structures and local magnetic moments in ferromagnetic and antiferromagnetic Fe<sub>x</sub>Rh<sub>1-x</sub> alloys, *J. Magn. Magn. Mater.* 66 (2) (1987) 175–186, [https://doi.org/10.1016/0304-8853\(87\)90290-3](https://doi.org/10.1016/0304-8853(87)90290-3). <http://www.sciencedirect.com/science/article/pii/0304885387902903>.
- [49] V.L. Moruzzi, P.M. Marcus, Antiferromagnetic-ferromagnetic transition in FeRh, *Phys. Rev. B* 46 (1992) 2864–2873, <https://doi.org/10.1103/PhysRevB.46.2864>. <http://link.aps.org/doi/10.1103/PhysRevB.46.2864>.
- [50] V.L. Moruzzi, P.M. Marcus, Giant magnetoresistance in FeRh: a natural magnetic multilayer, *Phys. Rev. B* 46 (1992) 14198–14200, <https://doi.org/10.1103/PhysRevB.46.14198>. <http://link.aps.org/doi/10.1103/PhysRevB.46.14198>.
- [51] C. Paduani, Magnetic properties of Fe–Rh alloys, *J. Appl. Phys.* 90 (12) (2001) 6251–6254, <https://doi.org/10.1063/1.1413708>. <https://doi.org/10.1063/1.1413708>.
- [52] L.M. Sandratskii, P. Mavropoulos, Magnetic excitations and femtomagnetism of FeRh: a first-principles study, *Phys. Rev. B* 83 (2011) 174408, <https://doi.org/10.1103/PhysRevB.83.174408>. <http://link.aps.org/doi/10.1103/PhysRevB.83.174408>.
- [53] J.B. Staunton, R. Banerjee, M. dos Santos Dias, A. Deak, L. Szunyogh, Fluctuating local moments, itinerant electrons, and the magnetocaloric effect: compositional hypersensitivity of FeRh, *Phys. Rev. B* 89 (2014), 054427, <https://doi.org/10.1103/PhysRevB.89.054427>. <https://link.aps.org/doi/10.1103/PhysRevB.89.054427>.
- [54] J. Kudrnovský, V. Drchal, I. Turek, Physical properties of FeRh alloys: the antiferromagnetic to ferromagnetic transition, *Phys. Rev. B* 91 (2015), 014435, <https://doi.org/10.1103/PhysRevB.91.014435>. <http://link.aps.org/doi/10.1103/PhysRevB.91.014435>.
- [55] E. Mendieta-Tapia, T. Castán, Magnetocaloric and barocaloric responses in magnetovolumic systems, *Phys. Rev. B* 91 (2015) 224421, <https://doi.org/10.1103/PhysRevB.91.224421>. <http://link.aps.org/doi/10.1103/PhysRevB.91.224421>.
- [56] J. Barker, R.W. Chantrell, Higher-order exchange interactions leading to metamagnetism in FeRh, *Phys. Rev. B* 92 (2015), 094402, <https://doi.org/10.1103/PhysRevB.92.094402>. <http://link.aps.org/doi/10.1103/PhysRevB.92.094402>.
- [57] S. Poleysa, S. Mankovsky, D. Ködderitzsch, J. Minár, H. Ebert, Finite-temperature magnetism of FeRh compounds, *Phys. Rev. B* 93 (2016), 024423, <https://doi.org/10.1103/PhysRevB.93.024423>. <http://link.aps.org/doi/10.1103/PhysRevB.93.024423>.
- [58] U. Aschauer, R. Braddell, S.A. Brechbühl, P.M. Derlet, N.A. Spaldin, Strain-

- induced structural instability in FeRh, *Phys. Rev. B* 94 (2016), 014109, <https://doi.org/10.1103/PhysRevB.94.014109>. <http://link.aps.org/doi/10.1103/PhysRevB.94.014109>.
- [59] M. Wolloch, M.E. Gruner, W. Keune, P. Mohn, J. Redinger, F. Hofer, D. Suess, R. Podloucky, J. Landers, S. Salamon, F. Scheibel, D. Spoddig, R. Witte, B. Roldan Cuenya, O. Gutfleisch, M.Y. Hu, J. Zhao, T. Toellner, E.E. Alp, M. Siewert, P. Entel, R. Pentcheva, H. Wende, Impact of lattice dynamics on the phase stability of metamagnetic FeRh: bulk and thin films, *Phys. Rev. B* 94 (2016) 174435, <https://doi.org/10.1103/PhysRevB.94.174435>. <http://link.aps.org/doi/10.1103/PhysRevB.94.174435>.
- [60] J. Kim, R. Ramesh, N. Kioussis, Revealing the hidden structural phases of FeRh, *Phys. Rev. B* 94 (18) (2016), <https://doi.org/10.1103/PhysRevB.94.180407>, 180407(R).
- [61] A. Popescu, P. Rodriguez-Lopez, P.M. Haney, L.M. Woods, Thermally driven anomalous hall effect transitions in FeRh, *Phys. Rev. B* 97 (2018) 140407, <https://doi.org/10.1103/PhysRevB.97.140407>. <https://link.aps.org/doi/10.1103/PhysRevB.97.140407>.
- [62] M. Manekar, S.B. Roy, Reproducible room temperature giant magnetocaloric effect in Fe-Rh, *J. Phys. D Appl. Phys.* 41 (19) (2008) 192004, <https://doi.org/10.1088/0022-3727/41/19/192004>. <http://stacks.iop.org/0022-3727/41/i=19/a=192004>.
- [63] J. Cao, N.T. Nam, S. Inoue, H.Y.Y. Ko, N.N. Phuoc, T. Suzuki, Magnetization behaviors for FeRh single crystal thin films, *J. Appl. Phys.* 103 (7) (2008) 07F501, <https://doi.org/10.1063/1.2828812>. <https://aip.scitation.org/doi/10.1063/1.2828812>.
- [64] K.G. Sandeman, Magnetocaloric materials: the search for new systems, *Scripta Mater.* 67 (6) (2012) 566–571, <https://doi.org/10.1016/j.scriptamat.2012.02.045>. <https://www.sciencedirect.com/science/article/pii/S1359646212001595>.
- [65] E. Stern-Taulats, A. Planes, P. Lloveras, M. Barrio, J.-L. Tamarit, S. Pramanick, S. Majumdar, C. Frontera, L. Mañosa, Baroclastic and magnetocaloric effects in Fe<sub>49</sub>Rh<sub>51</sub>, *Phys. Rev. B* 89 (2014) 214105, <https://doi.org/10.1103/PhysRevB.89.214105>. <http://link.aps.org/doi/10.1103/PhysRevB.89.214105>.
- [66] Y. Liu, L.C. Phillips, R. Mattana, M. Bibes, A. Barthélémy, B. Dkhil, Large reversible caloric effect in FeRh thin films via a dual-stimulus multicaloric cycle, *Nat. Commun.* 7 (2016) 11614, <https://doi.org/10.1038/ncomms11614>. <https://www.nature.com/articles/ncomms11614>.
- [67] J.A. Arregi, M. Horky, K. Fabianova, R. Tolley, E.E. Fullerton, V. Uhler, Magnetization reversal and confinement effects across the metamagnetic phase transition in mesoscale FeRh structures, *J. Phys. D Appl. Phys.* 51 (10) (2018) 105001, <https://doi.org/10.1088/1361-6463/aaa5a>. <http://iopscience.iop.org/article/10.1088/1361-6463/aaa5a>.
- [68] S.P. Bennett, A. Herklotz, C.D. Cress, A. Ilev, C.M. Rouleau, I.I. Mazin, V. Lauter, Magnetic order multilayering in FeRh thin films by He-ion irradiation, *Materials Research Letters* 6 (1) (2018) 106–112, <https://doi.org/10.1080/21663831.2017.1402098>.
- [69] P. Drózd, M. Ślęzak, K. Matlak, B. Matlak, K. Freindl, D. Wilgocka-Ślęzak, N. Spiridis, J. Korecki, T. Ślęzak, Switching of Co magnetization driven by antiferromagnetic-ferromagnetic phase transition of FeRh alloy in Co/FeRh bilayers, *Phys. Rev. Applied* 9 (2018) 034030, <https://doi.org/10.1103/PhysRevApplied.9.034030>. <https://link.aps.org/doi/10.1103/PhysRevApplied.9.034030>.
- [70] C. Cao, P. Li, W. Wang, W. Meng, J. Yao, C. Jiang, Y. Sivalingam, W. Han, A realization scheme of metamagnetic phase transition in FeRh films grown on glass substrates, *Appl. Surf. Sci.* 449 (4th International Conference on Nanoscience and Nanotechnology) (2018) 380–383, <https://doi.org/10.1016/j.apsusc.2017.12.059>. <http://www.sciencedirect.com/science/article/pii/S0169433217336462>.
- [71] J.-U. Thiele, S. Maat, E.E. Fullerton, FeRh/FePt exchange spring films for thermally assisted magnetic recording media, *Appl. Phys. Lett.* 82 (17) (2003) 2859–2861, <https://doi.org/10.1063/1.1571232>. <https://doi.org/10.1063/1.1571232>.
- [72] G. Ju, J. Hohlfield, B. Bergman, R.J.M. van de Veerdonk, O.N. Mryasov, J.-Y. Kim, X. Wu, D. Weller, B. Koopmans, Ultrafast generation of ferromagnetic order via a laser-induced phase transformation in FeRh thin films, *Phys. Rev. Lett.* 93 (2004) 197403, <https://doi.org/10.1103/PhysRevLett.93.197403>. <http://link.aps.org/doi/10.1103/PhysRevLett.93.197403>.
- [73] J.U. Thiele, S. Maat, J.L. Robertson, E.E. Fullerton, Magnetic and structural properties of FePt-FeRh exchange spring films for thermally assisted magnetic recording media, *IEEE Trans. Magn.* 40 (4) (2004) 2537–2542, <https://doi.org/10.1109/TMAG.2004.829325>.
- [74] R. Fan, C.J. Kinane, T.R. Charlton, R. Dorner, M. Ali, M.A. de Vries, R.M.D. Brydson, C.H. Marrows, B.J. Hickey, D.A. Arena, B.K. Tanner, G. Nisbet, S. Langridge, Ferromagnetism at the interfaces of antiferromagnetic FeRh epilayers, *Phys. Rev. B* 82 (2010) 184418, <https://doi.org/10.1103/PhysRevB.82.184418>. <http://link.aps.org/doi/10.1103/PhysRevB.82.184418>.
- [75] R.O. Cherifi, V. Ivanovskaya, L.C. Phillips, A. Zobelli, I.C. Infante, E. Jacquet, V. Garcia, S. Fusil, P.R. Briddon, N. Guiblin, A. Mouglin, A.A. Únal, F. Kronast, S. Valencia, B. Dkhil, A. Barthélémy, M. Bibes, Electric-field control of magnetic order above room temperature, *Nat. Mater.* 13 (4) (2014) 345–351, <https://doi.org/10.1038/nmat3870>. <https://www.nature.com/articles/nmat3870>.
- [76] X. Marti, I. Fina, C. Frontera, J. Liu, P. Wadley, Q. He, R.J. Paull, J.D. Clarkson, J. Kudrnovsky, I. Turek, J. Kunes, D. Yi, J.-H. Chu, C.T. Nelson, L. You, E. Arenholz, S. Salahuddin, J. Fontcuberta, T. Jungwirth, R. Ramesh, Room-temperature antiferromagnetic memory resistor, *Nat. Mater.* 13 (4) (2014) 367–374, <https://doi.org/10.1038/nmat3861>. <https://doi.org/10.1038/nmat3861>.
- [77] Z.Q. Liu, L. Li, Z. Gai, J.D. Clarkson, S.L. Hsu, A.T. Wong, L.S. Fan, M.-W. Lin, C.M. Rouleau, T.Z. Ward, H.N. Lee, A.S. Sefat, H.M. Christen, R. Ramesh, Full electroresistance modulation in a mixed-phase metallic alloy, *Phys. Rev. Lett.* 116 (2016) 097203, <https://doi.org/10.1103/PhysRevLett.116.097203>. <http://link.aps.org/doi/10.1103/PhysRevLett.116.097203>.
- [78] X. Zhou, F. Matthes, D.E. Bürgler, C.M. Schneider, Magnetic surface domain imaging of uncapped epitaxial FeRh(001) thin films across the temperature-induced metamagnetic transition, *AIP Adv.* 6 (1) (2016) 015211, <https://doi.org/10.1063/1.4940758>. <https://doi.org/10.1063/1.4940758>.
- [79] P. Carrillo, R. Shi, K. Teeluck, S.D. Senanayake, M.G. White, In situ formation of FeRh nanoalloys for oxygenate synthesis, *ACS Catal.* 8 (8) (2018) 7279–7286, <https://doi.org/10.1021/acscatal.8b02235>. <https://doi.org/10.1021/acscatal.8b02235>.
- [80] N.A. Zarkevich, D.D. Johnson, FeRh ground state and martensitic transformation, *Phys. Rev. B* 97 (2018) 014202, <https://doi.org/10.1103/PhysRevB.97.014202>. <https://link.aps.org/doi/10.1103/PhysRevB.97.014202>.
- [81] N.A. Zarkevich, Structural database for reducing cost in materials design and complexity of multiscale computations, *Complexity* 11 (2006) 36–42, <https://doi.org/10.1002/cplx.20117>. <https://onlinelibrary.wiley.com/doi/abs/10.1002/cplx.20117>.
- [82] J. Kübler, *Theory of Itinerant Electron Magnetism*, Clarendon Press, 2009.
- [83] S.V. Vonsovsky, *Magnetism*, Nauka, Moscow, 1971.
- [84] C. Toher, J.J. Plata, O. Levy, M. de Jong, M. Asta, M.B. Nardelli, S. Curtarolo, High-throughput computational screening of thermal conductivity, Debye temperature, and Grüneisen parameter using a quasiharmonic Debye model, *Phys. Rev. B* 90 (2014) 174107, <https://doi.org/10.1103/PhysRevB.90.174107>. <https://link.aps.org/doi/10.1103/PhysRevB.90.174107>.
- [85] S. Nikitin, G. Myalikgulyev, M. Annaorazov, A. Tyurin, R. Myndyev, S. Akopyan, Giant elastocaloric effect in FeRh alloy, *Phys. Lett.* 171 (1992) 234–236, [https://doi.org/10.1016/0375-9601\(92\)90432-L](https://doi.org/10.1016/0375-9601(92)90432-L). <https://www.sciencedirect.com/science/article/pii/037596019290432L>.
- [86] M.J. Richardson, D. Melville, J.A. Ricodreau, Specific heat measurements on an Fe-Rh alloy, *Phys. Lett.* 46 (1973) 153–154, <https://www.sciencedirect.com/journal/physics-letters-a/issue/2>.
- [87] G. Kresse, J. Hafner, Ab initio molecular dynamics for liquid metals, *Phys. Rev. B* 47 (1993) 558–561, <https://doi.org/10.1103/PhysRevB.47.558>. <https://link.aps.org/doi/10.1103/PhysRevB.47.558>.
- [88] G. Kresse, J. Hafner, Ab initio molecular-dynamics simulation of the liquid-metal – amorphous-semiconductor transition in germanium, *Phys. Rev. B* 49 (1994) 14251–14269, <https://doi.org/10.1103/PhysRevB.49.14251>. <https://link.aps.org/doi/10.1103/PhysRevB.49.14251>.
- [89] P.E. Blöchl, Projector augmented-wave method, *Phys. Rev. B* 50 (1994) 17953–17979, <https://doi.org/10.1103/PhysRevB.50.17953>. <https://link.aps.org/doi/10.1103/PhysRevB.50.17953>.
- [90] G. Kresse, D. Joubert, From ultrasoft pseudopotentials to the projector augmented-wave method, *Phys. Rev. B* 59 (1999) 1758–1775, <https://doi.org/10.1103/PhysRevB.59.1758>. <https://link.aps.org/doi/10.1103/PhysRevB.59.1758>.
- [91] J.P. Perdew, K. Burke, M. Ernzerhof, Generalized gradient approximation made simple, *Phys. Rev. Lett.* 77 (1996) 3865–3868, <https://doi.org/10.1103/PhysRevLett.77.3865>. <http://link.aps.org/doi/10.1103/PhysRevLett.77.3865>.
- [92] S.H. Vosko, L. Wilk, M. Nusair, Accurate spin-dependent electron liquid correlation energies for local spin density calculations: a critical analysis, *Can. J. Phys.* 58 (8) (1980) 1200–1211, <https://doi.org/10.1139/p80-159>. <http://www.nrcresearchpress.com/doi/pdf/10.1139/p80-159>.
- [93] D.D. Johnson, Modified broyden's method for accelerating convergence in self-consistent calculations, *Phys. Rev. B* 38 (1988) 12807–12813, <https://doi.org/10.1103/PhysRevB.38.12807>. <https://link.aps.org/doi/10.1103/PhysRevB.38.12807>.
- [94] H.J. Monkhorst, J.D. Pack, Special points for Brillouin-zone integrations, *Phys. Rev. B* 13 (1976) 5188–5192, <https://doi.org/10.1103/PhysRevB.13.5188>. <https://link.aps.org/doi/10.1103/PhysRevB.13.5188>.
- [95] D.D. Johnson, D.M. Nicholson, F.J. Pinski, B.L. Gyorffy, G.M. Stocks, Density-functional theory for random alloys: total energy within the coherent-potential approximation, *Phys. Rev. Lett.* 56 (1986) 2088–2091, <https://doi.org/10.1103/PhysRevLett.56.2088>. <http://link.aps.org/doi/10.1103/PhysRevLett.56.2088>.
- [96] D.D. Johnson, A.V. Smirnov, S.N. Khan, MECCA: Multiple-Scattering Electronic-Structure Calculations for Complex Alloys, KKR-CPA Program, Ver. 2.0, Iowa State University and Ames Laboratory, Ames, 2015.
- [97] N.A. Zarkevich, D.D. Johnson, Reliable first-principles alloy thermodynamics via truncated cluster expansions, *Phys. Rev. Lett.* 92 (2004) 255702, <https://doi.org/10.1103/PhysRevLett.92.255702>. <https://link.aps.org/doi/10.1103/PhysRevLett.92.255702>.
- [98] D. Sheppard, P.H. Xiao, W. Chmielewski, D.D. Johnson, G. Henkelman, A generalized solid-state nudged elastic band method, *J. Chem. Phys.* 136 (2012) 074103, <https://doi.org/10.1063/1.3684549>.
- [99] N.A. Zarkevich, D.D. Johnson, C2NEB Source Code, 2014. [http://lib.d.ia.state.edu/ameslab\\_software/1/](http://lib.d.ia.state.edu/ameslab_software/1/).
- [100] N.A. Zarkevich, D.D. Johnson, Nudged-elastic band method with two climbing images: finding transition states in complex energy landscapes, *J. Chem. Phys.* 142 (2) (2015) 024106, <https://doi.org/10.1063/1.4905209>.

- <https://aip.scitation.org/doi/10.1063/1.4905209>.
- [101] D. Alfé, Phon: a program to calculate phonons using the small displacement method, *Comput. Phys. Commun.* 180 (2009) 2622–2633, <https://doi.org/10.1016/j.cpc.2009.03.010>.
  - [102] N.A. Zarkevich, D.D. Johnson, Coexistence pressure for a martensitic transformation from theory and experiment: revisiting the bcc-hcp transition of iron under pressure, *Phys. Rev. B* 91 (17) (2015) 174104, <https://doi.org/10.1103/PhysRevB.91.174104>, <https://journals.aps.org/prb/abstract/10.1103/PhysRevB.91.174104>.
  - [103] N.A. Zarkevich, D.D. Johnson, Magneto-structural transformations via a solid-state nudged elastic band method: application to iron under pressure, *J. Chem. Phys.* 143 (2015) 064707, <https://doi.org/10.1063/1.4927778>, <https://aip.scitation.org/doi/10.1063/1.4927778>.
  - [104] N.A. Zarkevich, ThermoPhonon Code, 2014. [http://lib.dr.iastate.edu/ameslab\\_software/2/](http://lib.dr.iastate.edu/ameslab_software/2/), [http://lib.dr.iastate.edu/ameslab\\_software/2/](http://lib.dr.iastate.edu/ameslab_software/2/).
  - [105] A. Togo, I. Tanaka, First principles phonon calculations in materials science, *Scripta Mater.* 108 (2015) 1–5, <https://doi.org/10.1016/j.scriptamat.2015.07.021>, <http://www.sciencedirect.com/science/article/pii/S1359646215003127>.
  - [106] N.A. Zarkevich, T.L. Tan, D.D. Johnson, First-principles prediction of phase-segregating alloy phase diagrams and a rapid design estimate of their transition temperatures, *Phys. Rev. B* 75 (2007) 104203, <https://doi.org/10.1103/PhysRevB.75.104203>, <https://link.aps.org/doi/10.1103/PhysRevB.75.104203>.
  - [107] A. Alam, B. Kraczek, D.D. Johnson, Structural, magnetic, and defect properties of Co-Pt-type magnetic-storage alloys: density-functional theory study of thermal processing effects, *Phys. Rev. B* 82 (2010) 024435, <https://doi.org/10.1103/PhysRevB.82.024435>, <https://link.aps.org/doi/10.1103/PhysRevB.82.024435>.
  - [108] O. Bogdanoff, B. Fultz, Vibrational entropies of alloying and compound formation: experimental trends, *Phil. Mag. B* 79 (1999) 180407(R), <https://doi.org/10.1080/13642819908205747>, <https://www.tandfonline.com/doi/abs/10.1080/13642819908205747>.
  - [109] O. Delaire, B. Fultz, Charge redistribution and phonon entropy of vanadium alloys, *Phys. Rev. Lett.* 97 (2006) 245701, <https://doi.org/10.1103/PhysRevLett.97.245701>, <https://doi.org/10.1103/PhysRevLett.97.245701>.
  - [110] N.A. Zarkevich, First-principles Prediction of Thermodynamics and Ordering in Metallic Alloys, Ph.D. thesis, University of Illinois at Urbana-Champaign, 2003. <http://hdl.handle.net/2142/34849>.
  - [111] N. Zarkevich, D. Johnson, A. Smirnov, Structure and stability of hcp bulk and nano-precipitated Ag<sub>2</sub>Al, *Acta Mater.* 50 (9) (2002) 2443–2459, [https://doi.org/10.1016/S1359-6454\(02\)00075-7](https://doi.org/10.1016/S1359-6454(02)00075-7), <http://www.sciencedirect.com/science/article/pii/S1359645402000757>.
  - [112] N.A. Zarkevich, D.D. Johnson, Predicted hcp Ag-Al metastable phase diagram, equilibrium ground states, and precipitate structure, *Phys. Rev. B* 67 (2003) 064104, <https://doi.org/10.1103/PhysRevB.67.064104>, <https://link.aps.org/doi/10.1103/PhysRevB.67.064104>.
  - [113] N.A. Zarkevich, D.D. Johnson, Predicting enthalpies of molecular substances: application to LiBH<sub>4</sub>, *Phys. Rev. Lett.* 100 (2008) 040602, <https://doi.org/10.1103/PhysRevLett.100.040602>, <https://link.aps.org/doi/10.1103/PhysRevLett.100.040602>.
  - [114] D.D. Johnson, M. Asta, Energetics of homogeneously-random fcc al-ag alloys: a detailed comparison of computational methods, *Comput. Mater. Sci.* 8 (1–2) (1997) 54–63, [https://doi.org/10.1016/S0927-0256\(97\)00016-5](https://doi.org/10.1016/S0927-0256(97)00016-5).
  - [115] M. Asta, D.D. Johnson, Thermodynamic properties of fcc-based al-ag alloys, *Comput. Mater. Sci.* 8 (1–2) (1997) 64–70, [https://doi.org/10.1016/S0927-0256\(97\)00017-7](https://doi.org/10.1016/S0927-0256(97)00017-7).
  - [116] M. Asta, J.J. Hoyt, Thermodynamic properties of coherent interfaces in f.c.c.-based ag-al alloys: a first-principles study, *Acta Mater.* 48 (5) (2000) 1089–1096, [https://doi.org/10.1016/S1359-6454\(99\)00412-7](https://doi.org/10.1016/S1359-6454(99)00412-7), <http://WOS:000085932200007>.
  - [117] B. Schonfeld, J. Traube, G. Kosterz, Short-range order and pair potentials in au-ag, *Phys. Rev. B* 45 (2) (1992) 613–621, <https://doi.org/10.1103/PhysRevB.45.613>, <https://link.aps.org/doi/10.1103/PhysRevB.45.613>.
  - [118] V. Ozoliņš, C. Wolverton, A. Zunger, Cu-au, ag-au, cu-ag, and ni-au intermetallics: first-principles study of temperature-composition phase diagrams and structures, *Phys. Rev. B* 57 (1998) 6427–6443, <https://doi.org/10.1103/PhysRevB.57.6427>, <https://link.aps.org/doi/10.1103/PhysRevB.57.6427>.
  - [119] V. Ozoliņš, C. Wolverton, A. Zunger, First-principles theory of vibrational effects on the phase stability of cu-au compounds and alloys, *Phys. Rev. B* 58 (1998) R5897–R5900, <https://doi.org/10.1103/PhysRevB.58.R5897>, <https://link.aps.org/doi/10.1103/PhysRevB.58.R5897>.
  - [120] R. Hultgren, R.L. Orr, P.D. Anderson, K.K. Kelley, Selected Values of Thermodynamic Properties of Metals and Alloys, Wiley and Sons, 1963.
  - [121] H. Okamoto (Ed.), Desk Handbook: Phase Diagram for Binary Alloys, second ed., ASM International, 2010.
  - [122] A. Alam, B. Kraczek, D.D. Johnson, Structural, magnetic, and defect properties of Co-Pt-type magnetic-storage alloys: density-functional theory study of thermal processing effects, *Phys. Rev. B* 82 (2010) 024435, <https://doi.org/10.1103/PhysRevB.82.024435>, <https://link.aps.org/doi/10.1103/PhysRevB.82.024435>.
  - [123] ASM alloy phase diagrams database, <https://matdata.asminternational.org/apd/>, 2018.
  - [124] L. Swartzendruber, The Fe-Rh (iron-rhodium) system, *Bulletin of Alloy Phase Diagrams* 5 (1984) 456, <https://doi.org/10.1007/BF02872896>.
  - [125] J.A. Ricardeau, D. Melville, Model of the antiferromagnetic-ferromagnetic transition in FeRh alloys, *J. Phys. F* 2 (2) (1972) 337, <https://doi.org/10.1088/0305-4608/2/2/024>, <http://stacks.iop.org/0305-4608/2/i=2/a=024>.
  - [126] R.C. Wayne, Pressure dependence of the magnetic transitions in Fe-Rh alloys, *Phys. Rev.* 170 (1968) 523–527, <https://doi.org/10.1103/PhysRev.170.523>, <https://link.aps.org/doi/10.1103/PhysRev.170.523>.
  - [127] H. Yibole, A. Pathak, Y. Mudryk, F. Guillou, N. Zarkevich, S. Gupta, V. Balema, V. Pecharsky, Manipulating the stability of crystallographic and magnetic sub-lattices: a first-order magnetoelastic transformation in transition metal based laves phase, *Acta Mater.* 154 (2018) 365–374, <https://doi.org/10.1016/j.actamat.2018.05.048>, <http://www.sciencedirect.com/science/article/pii/S1359645418304154>.
  - [128] F. Scheibel, T. Gottschall, A. Taubel, M. Fries, K.P. Skokov, A. Terwey, W. Keune, K. Ollefs, H. Wende, M. Farle, M. Acet, O. Gutfleisch, M.E. Gruner, Hysteresis design of magnetocaloric materials – from basic mechanisms to applications, *Energy Technol.* 6 (8) (2018) 1397–1428, <https://doi.org/10.1002/ente.201800264>, <https://onlinelibrary.wiley.com/doi/abs/10.1002/ente.201800264>.
  - [129] J. Cui, Y.S. Chu, O.O. Famodu, Y. Furuya, J. Hattrick-Simpers, R.D. James, A. Ludwig, S. Thienhaus, M. Wuttig, Z. Zhang, I. Takeuchi, Combinatorial search of thermoelastic shape-memory alloys with extremely small hysteresis width, *Nat. Mater.* 5 (2006) 286, <https://doi.org/10.1038/nmat1593>.
  - [130] H. Jonsson, G. Mills, K.W. Jacobsen, Nudged Elastic Band Method for Finding Minimum Energy Paths of Transitions, World Scientific, 1998.
  - [131] H.N. Bez, A.K. Pathak, A. Biswas, N.A. Zarkevich, V. Balema, Y. Mudryk, D.D. Johnson, V.K. Pecharsky, Giant enhancement of the magnetocaloric response in Ni-Co-Mn-Ti by rapid solidification, *Acta Mater.* 173 (2006) 225–230, <https://doi.org/10.1016/j.actamat.2019.05.004>, <http://www.sciencedirect.com/science/article/pii/S1359645419302745>.
  - [132] A. Biswas, A.K. Pathak, N.A. Zarkevich, X. Liu, Y. Mudryk, V. Balema, D.D. Johnson, V.K. Pecharsky, Designing Room Temperature Giant Magnetocaloric Materials, in Preparation, 2019.
  - [133] U.S. Department of Energy, Office of Energy Efficiency and Renewable Energy, Energy Materials Network, <https://www.energy.gov/eere/energy-materials-network/>.